Direct and precursor-mediated hyperthermal abstractive chemisorption of Cl_2/Al(111)

G. C. Poon, T. J. Grassman, J. C. Gumy, and A. C. Kummel
Department of Chemistry and Biochemistry, University of California, San Diego, La Jolla, California 92093

(Received 18 February 2003; accepted 11 August 2003)

Resonantly enhanced multiphoton ionization (REMPI) and time-of-flight mass spectroscopy have been used to demonstrate that the reaction of Cl_2 on the low work function Al(111) surface proceeds via a prompt vertical electron harpooning process. Sticking measurements were performed showing that Cl_2 adsorbs via a direct chemisorption process at either high incident translation energy or high surface temperature. However, at glancing incident angles and low surface temperatures (100 K), a precursor-mediated channel predominates. REMPI studies show that fast abstracted Cl was produced via both channels: direct, remotely-dissociated incident Cl_2, and indirect, precursor-mediated Cl_2. For incident Cl_2 of 0.11 and 0.27 eV at 40° incident angle and 100 K surface temperature, only the precursor-mediated channel was observed with atomic Cl abstracted product energies of 0.09–0.14 eV. At high surface temperature, 500 K, all incident translational energies and angles yield only the direct channel, with abstracted product energies of 0.19–0.26 eV.
 [DOI: 10.1063/1.1615471]

I. INTRODUCTION

The reaction of Cl_2 with Al(111) involves vertically nonadiabatic charge transfer, remote dissociation, and high velocity neutral atom ejection via direct and precursor-mediated abstractive chemisorption. Kasemo and co-workers[1] first explored photon and electron emission from halogen/sodium systems. The theoretical groundwork for understanding the mechanism of nonadiabatic charge transfer between diatomic halogens and alkali-metal dimers and surfaces was proposed by Nørskov, Newns, and Lundqvist (NNL).[2] Since then, many similar systems involving electron harpooning and photon emission,[1,3–7] electron emission,[1,7–14] or direct electronic excitation[15] have been studied and reviewed.[16–18] The experimental work of Hellberg *et al.*[10] has demonstrated that the reaction of Cl_2 on the potassium surface involves electron harpooning, in direct support of the model proposed by NNL. As the Cl_2 approaches the surface, the effective vertical electron affinity becomes larger than the work function of the substrate; therefore, an electron can be transferred from the surface to the Cl_2. Image charge acceleration of the Cl_2^- anion toward the surface and fast dissociation of the molecule ensue, resulting in a neutral Cl and an anionic Cl^- near the surface. Subsequent transfer of a second electron to the neutral Cl can result in energetic exoelectron emission via an Auger relaxation, provided the neutral affinity level lies sufficiently below the potassium conduction band. After the process is complete, two Cl atoms are bound to the surface. The measured Auger exoelectron yield bears information of the dynamics at the surface. However, the authors did not note any substantial Cl^- anion ejection.

In addition to photon and electron emission, another observable that provides information upon chemical dynamics at the surface includes the ejection of neutrals.[19–22] The measured velocity of ejected atoms contains information about the transfer of the first electron. This is in contrast to exoelectron emission data, which mainly contains information about the transfer of the second electron. Our work shows that vertical electron transfer is the mechanism describing the reaction of Cl_2 with Al(111) at low coverage, producing hyperthermal ejection of neutral Cl atoms. The hyperthermal Cl atom ejection from this system is consistent with the NNL model.[2]

A heuristic model demonstrating the evolution of the Cl_2 and Cl_2^- potential energy curve system as the Cl_2 approaches the Al(111) surface is presented in Fig. 1. In Fig. 1(a), the Cl_2 is infinitely separated from the surface; in Fig. 1(d), the Cl_2 is <1.1 Å from the surface. The adiabatic electron affinity is the energy difference of a transition from the Cl_2 potential minimum to the Cl_2^- potential minimum. The work function of Al(111) (Φ_{Al}), the energy needed to liberate an electron from the Fermi sea at the Al(111) surface, is ~4.25 eV.[23]

At infinite separation [Fig. 1(a)] between the Cl_2 molecule and the Al(111) surface, the shape of the potentials for Cl_2 and Cl_2^- can be accurately described by gas phase potentials. However, to describe the interaction of the molecule with the surface, the gas phase Cl_2^- potential[17] must be shifted upward in energy by the work function of the Al(111) surface. Therefore, at infinite separation, the energy required to transfer an electron from Al(111) to Cl_2 is $\Phi_{Al}+E^A_{gas}$ [Eq. (1)],

$$\Phi_{Al}(\mathrm{eV})+E^A_{gas}(\mathrm{eV})=4.25\ \mathrm{eV}-3.00\ \mathrm{eV}=1.25\ \mathrm{eV}. \tag{1}$$

An adiabatic electron transfer at infinite separation is endothermic by 1.25 eV in the Cl_2/Al(111) system.

Closer to the surface (~2.9 Å), the Cl_2^- curve is shifted to lower energy by the image charge stabilization of Cl_2^-.

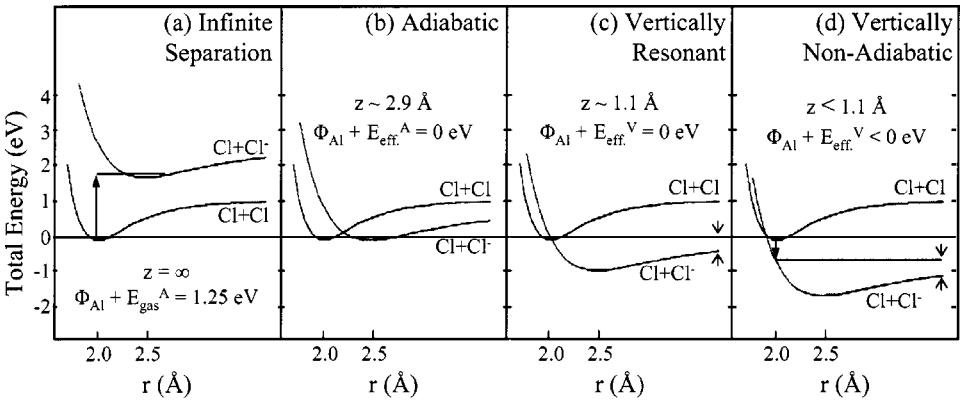

FIG. 1. Evolution of Cl_2 and Cl_2^- potential energy curves as a function of the Cl_2/Al(111) reaction coordinate (z). The separation between the Cl_2 and the surface (z) decreases from the left frame (a) to the right frame (d). (a) Adiabatic charge transfer is endothermic by 1.25 eV at infinite separation. (b) At $z \sim 2.9$ Å, the wave function overlap predicts small resonant adiabatic charge transfer probability. (c) At $z \sim 1.1$ Å, vertically resonant charge transfer results in dissociation of Cl_2^- into Cl and Cl^- fragments with the excess translational energy shown between the arrows. (d) At $z < 1.1$ Å, vertically nonadiabatic charge transfer results in the same products and excess energy as the vertically resonant process.

Using a simple jellium model, it has been shown that the image charge increases the adiabatic electron affinity by $-3.6\,\mathrm{eV}/z\,(\text{Å})$, where z is the distance between the molecule and the surface in angstroms.[17] This image charge shifted adiabatic electron affinity is termed the effective adiabatic electron affinity (E_{eff}^A). Horizontally adiabatic charge transfer from the Cl_2 potential minimum to the Cl_2^- potential minimum is shown in Fig. 1(b). This process would require the Cl–Cl bond to stretch on a time scale on the order of the electronic transition. This assumption is not valid: an electronic transition would be much faster than the bond length relaxation. In this case, the Franck–Condon overlap of the Cl_2 and Cl_2^- wave functions predicts only a small probability for adiabatic charge transfer.

The high incident velocity allows the Cl_2 to move closer to the surface shifting the Cl_2^- curve to even lower energies, again due to image charge stabilization of Cl_2^-, shown in Figs. 1(c) and 1(d). In Fig. 1(c), the Cl_2 is sufficiently close to the surface that the Cl_2^- potential crosses the Cl_2 potential at the Cl_2 potential minimum. The vertical electron affinity is the energy difference between the Cl_2 potential minimum and the Cl_2^- potential at constant internuclear separation ($\Delta r = 0$). The vertical electron affinity is shifted by $-3.6\,\mathrm{eV}/z\,(\text{Å})$ near the surface due to Cl_2^- image charge stabilization. This shifted vertical electron affinity is termed the effective vertical electron affinity of the Cl_2 (E_{eff}^V). When the molecule is sufficiently close to the surface that the effective vertical electron affinity is equal to the work function of the metal ($|E_{\mathrm{eff}}^V| = \Phi_{\mathrm{Al}}$), a Franck–Condon allowed harpooning event can occur. The distance at which the electron harpoons from the surface to the Cl_2 can be calculated using Eq. (2),[17]

$$z_{\mathrm{harpooning}} = \frac{3.6\ \text{Å}}{\Phi_{\mathrm{Al}}(\mathrm{eV}) + E_{\mathrm{gas}}^V(\mathrm{eV})}. \tag{2}$$

Using this equation, a vertically resonant harpooning distance between the assumed jellium sea and the assumed hole of 1.1 Å is calculated.

After the charge transfer, the Cl_2^- is formed high on the repulsive portion of its potential. The Cl–Cl bond immediately begins to extend from 1.99 Å (Cl_2) to 2.47 Å (Cl_2^-). The total energy of the Cl_2^- system resides above the dissociation limit of Cl_2^-. A portion of the excess energy, $E_{\mathrm{excess}}(Cl_2^-) = E_{\mathrm{after\ harpoon}}(Cl_2^-) - E_{\mathrm{vacuum}}(Cl_2^-)$, can be channeled into the translational energy of a departing Cl atom.

The most likely scenario leading to hyperthermal Cl atom ejection is a vertically nonadiabatic [Fig. 1(d)] charge transfer. The Cl_2–surface distance at which vertically resonant charge transfer occurs can be seen as the threshold for a vertical charge transfer ($|E_{\mathrm{eff}}^V| = \Phi_{\mathrm{Al}}$): it is the furthest distance at which an electron can harpoon. The high velocity of the incident Cl_2 may allow it to approach passed this threshold, creating a highly excited hole at the surface. In the vertically nonadiabatic charge transfer, the effective vertical electron affinity of the Cl_2 exceeds the work function of the Al(111) surface ($|E_{\mathrm{eff}}^V| > \Phi_{\mathrm{Al}}$). Similar to the case of vertically resonant charge transfer, excess energy can be channeled into the translational energy of a departing Cl atom. Using simple gas phase potentials of Cl_2 and Cl_2^-,[17] we estimate a total excess energy of 0.4 eV for either vertically resonant or vertically nonadiabatic charge transfer [Fig. 1(c) or 1(d)]. Assuming equal partitioning of this energy into each Cl atom, the velocity of the ejected Cl atom is estimated to be 1050 m/s. This simple calculation does not take into regard factors such as incident translational energy, molecular orientation of the impingent Cl_2, acceleration of the anion upon harpooning, etc.

The differentiation between vertically resonant and vertically nonadiabatic charge transfer is indeed difficult. The vertical transition from the Cl_2 potential to the Cl_2^- potential places the molecule at the same position high on the repulsive portion of the anion potential for both processes, resulting in the same predicted exit translational energy of the ejected Cl atom. The observation of hyperthermal Cl ejection from the surface would indicate that electron harpooning occurs at low coverage; the distinction between vertically reso-

nant and vertically nonadiabatic charge transfer processes is not particularly relevant.

Initial sticking probability on the surface is measured using two different King and Wells-type sticking techniques. Three sets of time-of-flight experiments determine the velocity of ejected Cl atoms from the reaction of Cl_2 on the Al(111) surface. Both a direct and a precursor-mediated channel produce hyperthermal product. Using a normal incident Cl_2 beam, ejected Cl velocities are measured at three exit angles to show the existence of hyperthermal product ejection. Further experiments performed by varying the incident angle and surface temperature are used to differentiate the direct channel from the precursor-mediated channel.

II. EXPERIMENTAL SET-UP

The reaction dynamics of Cl_2 on Al(111) are studied using time-of-flight mass spectroscopy (TOF-MS) with resonantly enhanced multiphoton ionization (REMPI) of scattered atomic chlorine under ultrahigh vacuum (UHV) conditions. The details of the experimental apparatus have been previously published.[24–27] The set-up for the current experiments includes a tunable light source with a complementary TOF-MS for the detection of ionized incident and scattered product species. The molecular beam source consists of a differentially pumped pulsed valve supersonic Cl_2 molecular beam directed into the ultrahigh vacuum reaction chamber with a base pressure of 1.8×10^{-10} Torr. A standard suite of UHV instruments is also available, including an argon ion sputter gun, a quadrupole mass spectrometer (QMS), an Auger electron spectrometer (AES), and a low-energy electron diffractometer (LEED).

REMPI is used to ionize the atomic $\mathrm{Cl}\,3p\,^2P_{3/2} \rightarrow 4p'\,^2F_{7/2}$ transition at 210.1 nm.[28–31] The doubled output (532 nm) of a Q-switched Nd:YAG laser (Quantel 581 C-SF) pumps a DCM dye laser (Lambda Physik FL-3002). The 630.3 nm fundamental (Lambda Physik DCM/Fisher Optima methanol) from the dye laser is doubled in KDP-C then tripled in BBO-1, using a pair of Inrad Autotracker III's, to obtain the desired 210.1 nm UV light. The 210.1 nm UV is isolated from the dye fundamental and doubled frequencies using dichroic mirrors and subsequently sent into the reaction chamber. A 370 mJ, 532 nm pulse from the Nd:YAG laser produces 55 mJ of 630.3 nm dye fundamental and 1.5 mJ of 210.1 UV, with pulse widths of <7 ns.

Using a 20 cm focal length lens, the laser is focused into the chamber in an orientation orthogonal to the molecular beam path. The lens is mounted off axis in a rotable barrel which allows the laser focus to be positioned in the molecular beam path or rotated in an arc around the dose spot on the sample for angular dependent detection of scattered products. The diameter of the arc (1.41 ± 0.03 cm) of the laser focus is controlled by the radial position of the lens from the center axis of the barrel. For experiments reported in this manuscript, the detection laser is rotated from 15° to 35° relative to normal incidence.

The skimmed and chopped (~15 μs pulse width, 10 Hz) diatomic chlorine molecular beam is created using a pulsed valve (General Valve, model 9-400-900 2 mm orifice) in a triple differentially pumped source chamber and directed at the surface at three incident kinetic energies: pure Cl_2 (0.11 ± 0.02 eV), Cl_2 seeded in Ne (0.27 ± 0.01 eV), and Cl_2 seeded in He (0.65 ± 0.01 eV). Chlorine is purchased premixed with He (Cl_2 5.32%/He balance) and Ne (Cl_2 5%/Ne balance) from Matheson. Pure chlorine is also purchased from Matheson. No contamination by other halogens is detected by QMS.

Standard surface preparation techniques are employed to clean and characterize the Al(111) surface. The surface is prepared by 2 kV Ar^+ ion sputtering followed by electron beam annealing at 773 K for 2 min. The surface dosing follows immediately after verification of cleanliness by AES. Surface order is checked by LEED.

The Al(111) crystal is maintained at one of three temperatures by cooling the surface to 100 ± 3 K using liquid nitrogen, cooling to room temperature (300 ± 3 K) using an air line, or heating to 500 ± 5 K using radiative heating. Three surface orientations (0°,20°,40°) with respect to the incident beam are used. Varying the surface temperature and orientation allows for differentiation between the direct and precursor-mediated abstractive chemisorption mechanism for Cl_2 on Al(111).

A thermionics time-of-flight mass spectrometer is mounted on a rotable flange. The spectrometer is a standard two grid accelerator, two-pole aspherical lens steered TOF-MS. The length of the flight tube is 10 cm. The TOF-MS is tilted toward the surface (45°) to maximize the signal of the scattered products.

The velocity of the incident beam from the chopper to the surface (v_{CS}) is measured using a UTI 100C quadrupole mass spectrometer. The TOF and pulse profile of the incident Cl_2 is measured daily using the laser TOF-MS method. These checks are performed to verify that the incident velocity is consistent with the QMS value and to ensure that the arrival time of the incident Cl_2 at the surface (t_{CS}) is consistent between experiments. For example, the t_{CS} of the incident Cl_2/He is 116.7 ± 0.3 μs for 19 random samples, indicating that we have experimental control of the incident beam. This time (t_{CS}) is the zero time of the ejected product time-of-flight. The window of ion collection for the determination of product velocities is at most 50 μs from t_{CS}. No signal is seen after 6 ms. We are not able to measure long lived precursors since any long-lived desorption states would have negligibly small signals. For example, if the precursor lifetime was 5 ms, the precursor desorption signal would be 100 times smaller than the scattered signal and therefore undetectable.

The initial sticking probability of Cl_2 on Al(111) is measured using two King and Wells-type sticking experiments. For both experiments, a movable Pyrex flag is used to block the molecular beam both prior to and after surface dosing. A gate valve blocks the molecular beam for background measurements. A standard sticking experiment set-up uses the QMS analog output to a National Instruments LabView Virtual Instrument to monitor the partial pressure of Cl_2. A peak-to-peak sticking experiment is performed using a QMS and a Tektronix TDS 3052 oscilloscope.

The velocity of the ejected Cl atoms is determined using the TOF of the neutral reaction products from the surface to

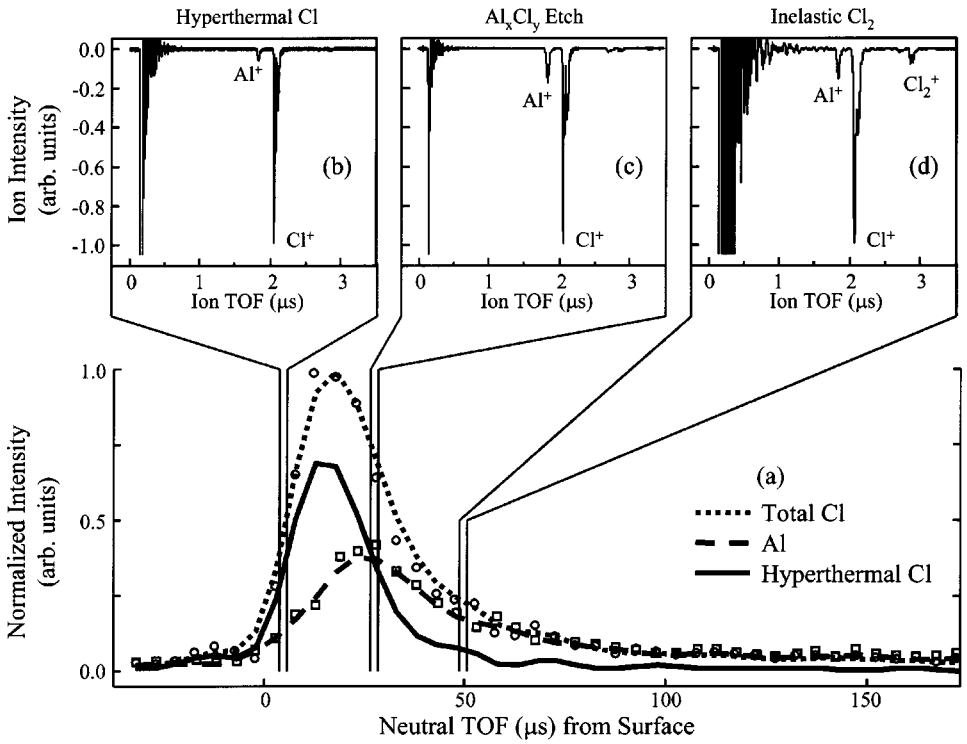

FIG. 2. Neutral TOF spectrum of total Cl^+ and Al^+ and a series of ion TOF-MS spectra taken at three selected TOF's from the surface: (b) $t_{neutral}=7\ \mu s$, (c) $t_{neutral}=29\ \mu s$, and (d) $t_{neutral}=50\ \mu s$. (a) The neutral TOF is representative of the data used for the Cl velocity measurements. The hyperthermal exit Cl signal is obtained by subtracting Al^+ signal from total Cl^+ signal. The ratio of integrated ion intensities (Al^+:Cl^+:Cl_2^+) at each $t_{neutral}$ are: (b) 22:310:1, no Cl_2 detected; (c) 10:50:1, maximum Al^+ signal; (d) 2:13:1; steady state etch and inelastically scattered Cl_2.

the laser focus. The distance from the surface dose spot to the detection laser is checked weekly.

III. RESULTS

Two different types of time-of-flight spectra characterize the scattered products. First, neutral TOF spectra are recorded by increasing the delay between the chopper trigger and the laser trigger by small increments (typically about 2–3 μs). These spectra quantify the flight time of the scattered products from the surface to the laser focus. Second, analysis of the ion TOF, defined as the flight time from the laser focus to the TOF-MS electron multiplier, probes the mass of the species present in the scattered signal.

Four distinct species constitute the observed scattered atomic chlorine TOF spectra. The contributions of each of these components to the total scattered Cl atom signal are independently characterized. The components include: Cl from aluminum chloride etch products [Eq. 3(a)], Cl from the photodissociation of inelastically scattered Cl_2 [Eq. 3(b)], direct abstracted Cl from remotely dissociated incident Cl_2, and indirect abstracted Cl from precursor-mediated chemisorption of Cl_2 [Eq. 3(c)]. We justify the proposed bimodal abstraction reaction of Cl_2 on Al(111) by confidently accounting for the etch products and inelastically scattered Cl_2,

$$\begin{aligned} &Al_2Cl_6 + xh\nu \rightarrow 2Al + 6Cl \\ &Al + xh\nu \rightarrow Al^+ \\ &Cl + (2+1)h\nu \rightarrow Cl^+ \end{aligned}, \tag{3a}$$

$$\begin{aligned} &Cl_2 + h\nu \rightarrow 2Cl \\ &Cl + (2+1)h\nu \rightarrow Cl^+, \end{aligned} \tag{3b}$$

$$Cl + (2+1)h\nu \rightarrow Cl^+. \tag{3c}$$

A. Etch

A typical neutral species TOF spectrum which displays normalized ion intensity vs flight time from the surface (μs) is shown in Fig. 2(a). The total Cl^+ signal (○) is predominantly composed of atomic chlorine from the direct harpooning and indirect precursor-mediated harpooning reactions along with photodissociated chlorine from the slower aluminum chloride etch products. The results of numerous research groups show that these etch products are primarily Al_2Cl_6 (below 450 K) and $AlCl_3$ (500–700 K).[32–37] A complementary Al^+ TOF spectrum (□) is recorded for each Cl signal. Because the MPI detection of Al^+ is much less efficient than the REMPI detection of Cl^+, the Al^+ signal is scaled to fit the Cl^+ signal at long times. At long times, both the Cl^+ and the Al^+ signals originate from etch products. Subtraction of the well-separated Al^+ etch signal from the total Cl^+ signal allows us to obtain the hyperthermal abstracted components of the Cl signal (solid line).

B. Inelastic

Several techniques determine that the source of Cl^+ signal originates predominately from atomic Cl, not from molecular Cl_2. At early arrival times [Fig. 2(b)], the ratio of atomic chlorine to molecular chlorine (Cl:Cl_2) is 310:1. A Cl:Cl_2 ratio of 50:1 is measured for molecular chlorine inelastically scattered from an inert aluminum oxide surface. This indicates that even with the most conservative estimates and the assumption that one count of Cl_2 signal results in 50 counts of atomic Cl in pure inelastically scattered Cl_2, a minimum of 80% of the atomic chlorine signal results solely from abstracted Cl product. Further data supports up to 95% hyperthermal Cl at early arrival times.

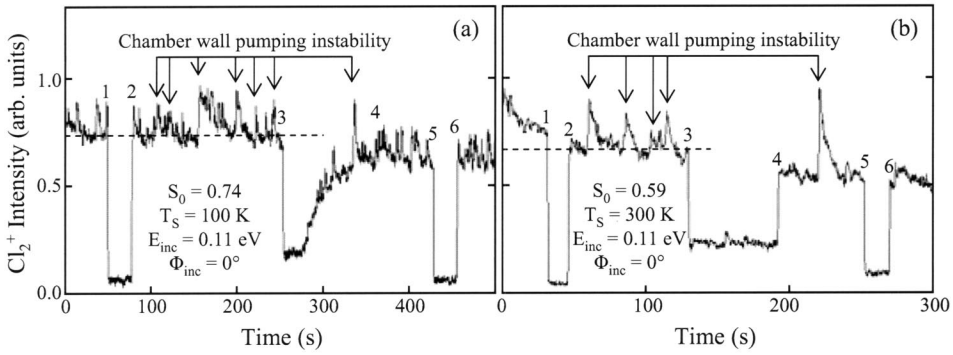

FIG. 3. Standard King and Wells sticking experiment. In both figures: (1) gate closed, (2) gate open, (3) flag open, (4) flag closed, (5) gate closed, and (6) gate open. Note the instability in the baseline due to chamber wall pumping. (a) At 100 K surface temperature and <0.2 eV Cl_2 incident energy, near unity initial sticking is expected; however, only 74% initial sticking is measured. Unusual bimodal sticking (a, 3–4) composed of instantaneous steady state sticking followed by saturation is attributed to chamber wall pumping. (b) For all other conditions, e.g., surface temperature=300 K and Cl_2 incident energy=0.11 eV, the sticking measurements exhibited nonsaturating steady state sticking (b, 3–4).

At both medium [Fig. 2(c), 30 μs] and long times [Fig. 2(d), 50 μs], only small amounts of inelastically scattered Cl_2 are detected. This detection proves that the apparatus is sensitive to Cl_2. However, this Cl_2 signal is sufficiently well-separated in time that it does not add appreciably to the atomic Cl signal seen at early times (<20 μs).

The incident angle of the molecular beam is also used to separate the inelastically scattered Cl_2 from the atomic Cl. At glancing incident angles, the detection of the inelastic collisions of Cl_2 on the Al(111) surface can be eliminated since the inelastically scattered products leave the surface at specular angles. The fast ejected Cl product should leave the surface along the surface normal, regardless of incident angle. Upon verification that the Cl velocities are nearly identical at forward and backscattering angles, we assert that the ejected Cl signal primarily arises from ejected Cl atoms and not from the photodissociation of inelastically scattered Cl_2.

C. Hyperthermal Cl product

1. Sticking experiment

Standard King and Wells reflection technique sticking experiments[38,39] using a QMS to monitor the partial pressure of Cl_2 exhibits very poor signal to noise because the chamber walls of the large reaction vessel act as efficient Cl_2 pumps. Upon exposing the surface to Cl_2, steady state sticking of only ~70% is initially seen at low surface temperature ($T_S = 100$ K) and low incident energy (<0.2 eV) followed by an abrupt transition to saturation of the surface [Fig. 3(a)]. The initial sticking measurements, under other conditions [$E_{inc}(Cl_2) = 0.11$ eV at $T_S \geqslant 300$ K or $E_{inc}(Cl_2) \geqslant 0.27$ eV at $T_S \geqslant 100$ K], behave as expected for continuous etching as shown in Fig. 3(b). For $E_{inc}(Cl_2) < 0.2$ eV at $T_S = 100$ K, we expect saturation starting when the flag is withdrawn [Fig. 3(a)]. Instead, the saturation has a 20 s induction time. Barenbak *et al.*[40] have observed this previously and ascribe it to desorption of gas from the chamber walls closest to the quartz flag. This indicates that the real sticking at $E_{inc}(Cl_2) < 0.2$ eV at $T_S = 100$ K is $>70\%$.

A transient peak-to-peak sticking method (Fig. 4) accommodates the fast pumping of Cl_2 between molecular beam pulses and accurately measures the sticking probability at low surface temperature and low incident energy. At all other surface temperatures and incident energies, the measured sticking is the same for both techniques providing the validity of the transient peak-to-peak method. The fast oscilloscope records the QMS signal while the molecular beam is run at 2 or 5 Hz to lower the dose rate. Several peaks, taken while the flag blocks the beam path (Fig. 4. 1–6), are averaged to obtain a baseline for each run. Note the immediate decay of each peak, indicative of very fast chamber pump-

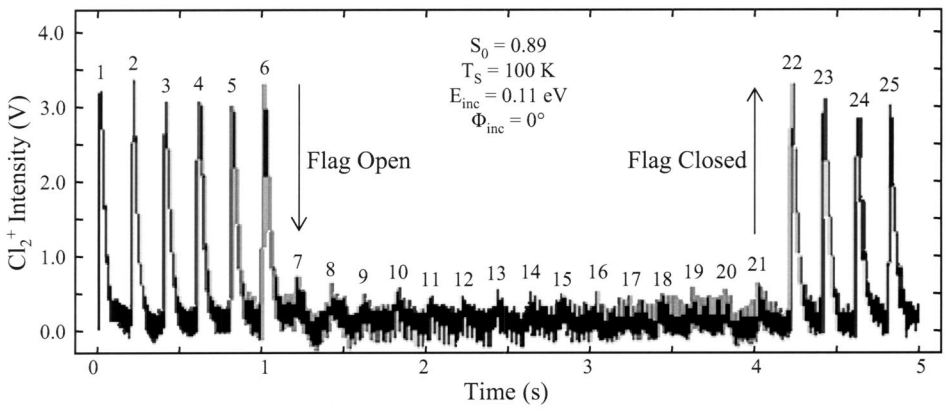

FIG. 4. Peak-to-peak King and Wells sticking experiment. Note the fast decay of the Cl_2 signal between 5 Hz molecular beam pulses. For the averaged peak-to-peak method, the three regimes parallel a standard KW experiment: flag in=background (1–6); flag out=surface exposed (7–21); and flag in=background (22–25). Signal amplitudes within each regime are averaged.

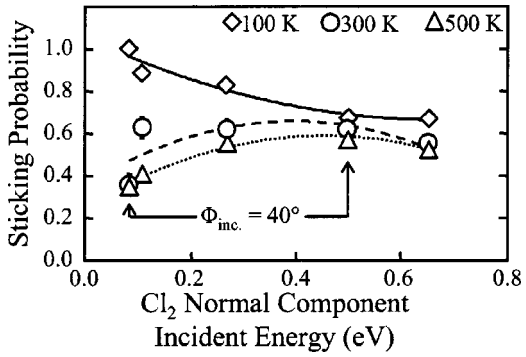

FIG. 5. Cl_2/Al(111) sticking probability as a function of surface temperature (T_S) and incident Cl_2 translational energy (E_{inc}). Normal incident translational energy is varied both by seed gas and surface tilt (Φ_{inc}). Sticking is enhanced at low incident translational energy (0.08–0.27 eV) and low surface temperature (100 K).

ing. The values for initial sticking after the flag is removed (Fig. 4. 7–21) and for background verification after the flag is replaced (Fig. 4. 22–25) are both obtained by a similar peak averaging method. A statistical analysis is made possible by multiple runs taken at each set of conditions.

The initial sticking probability vs surface temperature and incident kinetic energy (Fig. 5) supports the assertion that a precursor state exists at low surface temperature ($T_S = 100\,K$) and low incident energy $Cl_2(<0.2\,eV)$. The incident kinetic energy of the Cl_2 is varied by seed gas and by tilting the surface. For high incident energy Cl_2 (0.50–0.65 eV), the sticking probability is independent of surface temperature (~60%). At low incident energies, surface temperature gives rise to a pronounced effect: sticking probabilities between 20%–40% are measured at 300 and 500 K surface temperatures. However, low temperature and low incident kinetic energy conditions enhance the sticking to 80%–100%, indicating a molecular precursor.

2. Exit angle experiment

From the pure hyperthermal abstracted Cl product TOF spectra, velocities are obtained. The most probable arrival time is defined as half of the full width half maximum plus the arrival of the leading edge half maximum. The velocity of the ejected Cl atoms is measured as a function of (1) exit angle, (2) incident angle, and (3) surface temperature.

Our simple model predicts that the direct channel should produce ejected product along the surface normal and the velocity of the ejected Cl from the direct channel should be independent of incident Cl_2 kinetic energy. Detection of high velocity Cl along the surface normal is an indication of a vertical electron transfer process. Other factors which may influence the exit angle and energy of the ejected Cl include the orientation of the impinging Cl_2 molecule with respect to the surface normal, the acceleration of the Cl_2^- anion post harpooning, and the partitioning of the Cl_2^- dissociation energy. These will be discussed further in Sec. IV A.

Figure 6 shows the laser/surface orientations for the exit angle measurements. For these experiments, the high and low incident energy Cl_2 are directed along the surface normal and the laser focus lens is rotated to 15°, 22°, and 35°

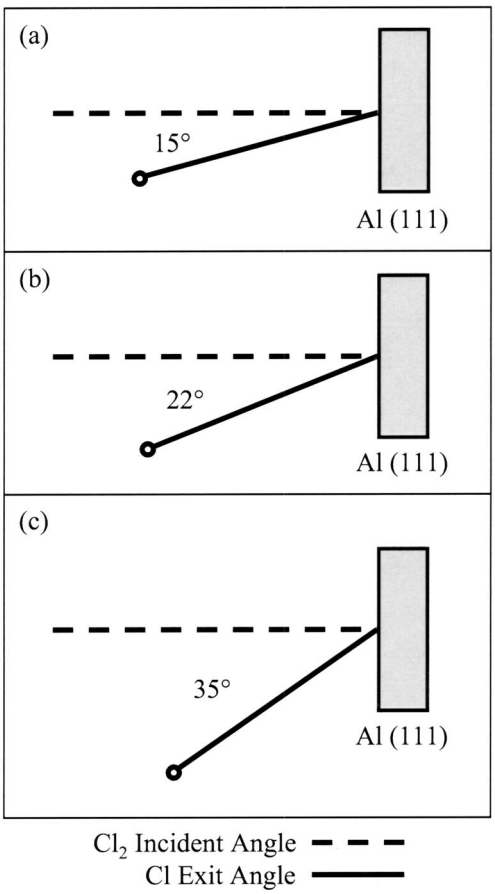

FIG. 6. The exit angle experiment includes three sets of incident angle (Φ_{inc})/exit angle (Φ_{exit}) laser focus orientations relative to the surface normal (a) 0°/15°, (b) 0°/22°, and (c) 0°/35°.

detection angles. Exactly normal detection of scattered product during normal incident dosing is impossible due to the large intensity of the incident beam; therefore, the detection laser is placed just outside of the incident beam (15° with respect to the surface normal).

The energy of abstracted Cl is independent of exit angle (15°–35°) and incident Cl_2 energy at 100 K surface temperature (Fig. 7, left axis, solid symbols). Incident Cl_2 beams of 0.11 eV (▲), 0.27 eV (●), and 0.65 eV (♦) all produce ejected Cl of 0.21 ± 0.03 eV. This observed Cl energy is nearly half of the 0.4 eV total excess energy estimated earlier using only simple gas phase potentials. This fortuitous result depends upon highly complex factors. However, the independence of the exit energy on the exit angle at near-normal exit angles is consistent with the simple model of electron harpooning shown in Fig. 1.

A plot of velocity vs exit angle (Fig. 7, right axis, open symbols) demonstrates the hyperthermicity of the ejected Cl. For all Cl_2 incident energies and exit angles, a mean velocity of 1045 ± 27 m/s is measured for 100 K Al(111). This mean was calculated using 68 samples and the error bound used is the standard error. The ratio of the mean product velocity vs the full width at half maximum (FWHM) of the TOF is a good metric upon the relative width of the velocity distribution. A thermal flux-weighted Maxwell–Boltzmann distribu-

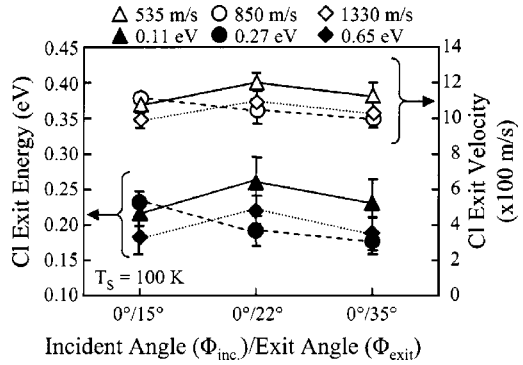

FIG. 7. Exit Cl translational energy (E_{exit}, left axis, solid symbols) and velocity (V_{exit}, right axis, open symbols) as a function of incident Cl_2 translational energy (E_{inc}) and velocity (V_{inc}), respectively, and exit angle (Φ_{exit}) at normal incidence ($\Phi_{inc}=00$) and low surface temperature (100 K). The measured E_{exit} is independent of E_{inc} and Φ_{inc}. Ejected Cl from Cl_2 beams impingent on the surface at 535 and 850 m/s are accelerated to ~1050 m/s.

tion exhibits a 1:1 ratio between the most probable velocity and the FWHM.[41] However, the mean velocity to FWHM of the 0.65 eV normal incident beam from a 500 K surface yielded a ratio of ~0.84, indicating a relatively broad velocity distribution. This ratio will be compared to the ratio found for the precursor channel in Sec. IV B. The mean velocity of Cl product exceeds the incident velocity of Cl_2/Ne and pure Cl_2 using all exit angles. For example, the velocities of the ejected Cl from incident Cl_2/Ne (850 m/s) and pure Cl_2 (535 m/s) are accelerated to 1006 and 1164 m/s, respectively. As explained in the Introduction, assuming a simple vertical transition between the gas phase Cl_2 and the work function/image shifted Cl_2^- potentials with equal partitioning of the excess energy into the two fragments, we estimate a Cl exit velocity of 1050 m/s. The experimental data is consistent with a vertical electron harpooning mechanism.

3. Fixed laser experiment

The surface/laser orientation for incident/exit angle and surface temperature experiments is shown in Fig. 8. For these experiments, the laser focus remains at 15° with respect to the incident molecular beam. The purpose of this experiment is to determine the effect of incident angle. As the surface is tilted from normal to 20° to 40°, detection at 15, −5°, and −25° exit angles is a consequence of fixing the laser focus.

Tilting the surface while holding the laser position fixed results in detection of the product at a backscattered angle, thereby reducing the sensitivity to inelastically scattered Cl_2. At 20° incidence [Fig. 8(b)], the detection angle is −5°, and at 40° incidence [Fig. 8(c)], the detection angle is −25°. The exit angle of hyperthermal products resulting from a nonadiabatic electron harpooning mechanism should not be a function of incident angle and should produce backscattered Cl.

Figure 9 shows the translational energy of the abstracted Cl product, E_{trans}(Cl), vs the translational energy of the incident Cl_2, E_{trans}(inc), at three sets of surface orientations and 100 K surface temperature. At 0°/15°, the exit translational energy (0.21±0.01 eV) of the ejected Cl atom is independent of incident kinetic energy (0.11–0.65 eV). At glancing incident angles (20° and 40°), the energy of the ejected Cl is less than for normal incident Cl_2 beams and the exit energy of the Cl is a function of incident energy. At 40° incident angle, 0.65 eV incident Cl_2 resulted in 0.17±0.01 eV, 0.27 eV incident Cl_2 resulted in 0.14±0.02 eV, and 0.11 eV incident Cl_2 resulted in 0.09±0.02 eV. Note that even for

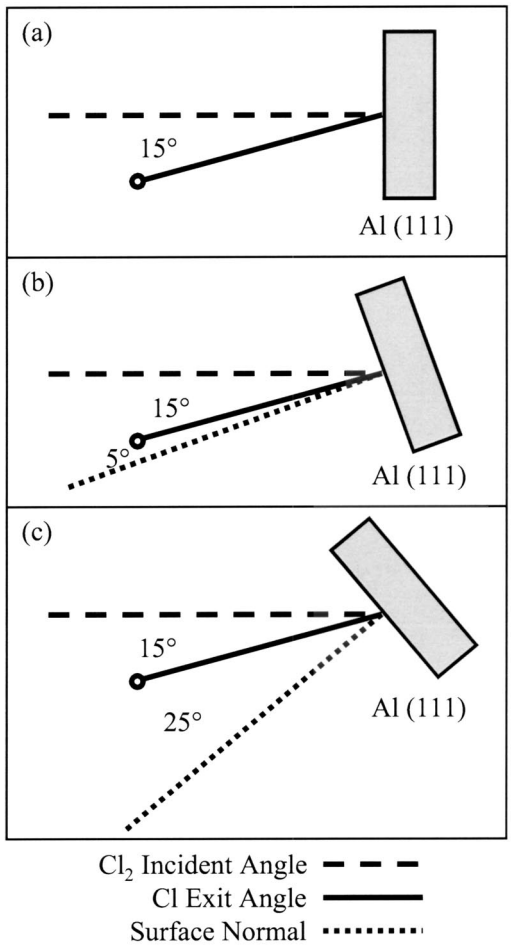

FIG. 8. The surface tilt experiment includes three sets of incident angle (Φ_{inc})/exit angle (Φ_{exit}) laser focus orientations with respect to the surface normal (a) 0°/15°, (b) 20°/−5°, and (c) 40°/−25°. A negative exit angle denotes detection at negative specular angles relative to the surface normal.

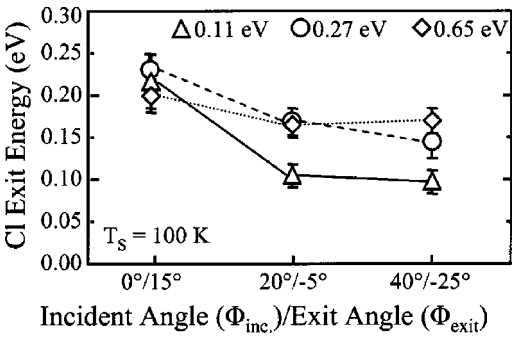

FIG. 9. Exit Cl translational energy (E_{exit}) as a function of incident Cl_2 translational energy (E_{inc}) and incident angle (Φ_{inc}) at low surface temperature (100 K). The measured E_{exit} decreases sharply at glancing Φ_{inc} (20° and 40°) for all E_{inc} consistent with a precursor-mediated channel.

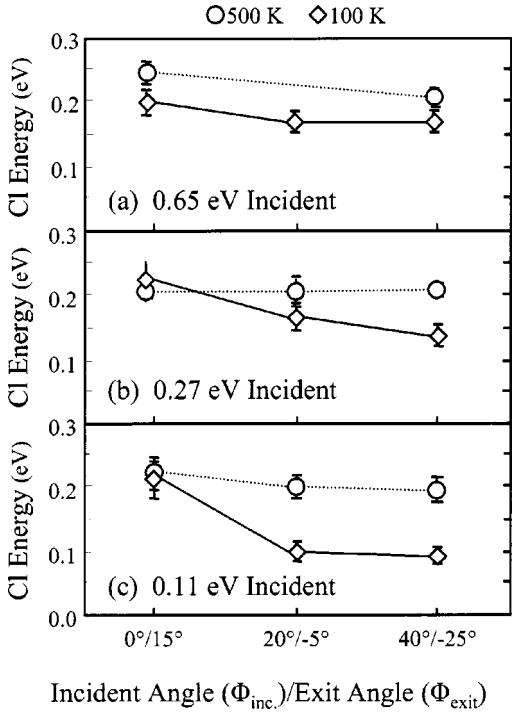

FIG. 10. Exit Cl translational energy (E_{exit}) as a function of incident Cl_2 translational energy (E_{inc}), incident angle (Φ_{inc}), and surface temperature (T_S). E_{exit} is a weak function of T_S for 0.65 eV E_{inc} Cl_2. For 0.11 eV and 0.27 eV E_{inc} Cl_2 at $\Phi_{inc}=20°$ and 40°, increasing T_S from 100 K to 500 K removes the low E_{exit} precursor channel.

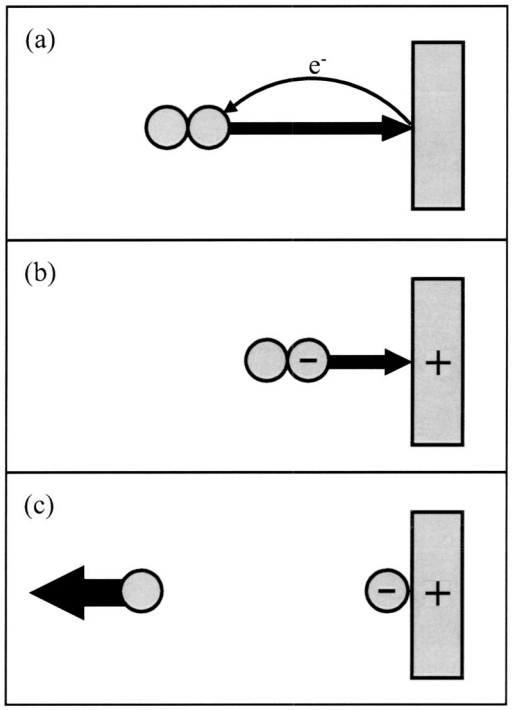

FIG. 11. Schematic diagram of direct, vertical electron transfer. (a) Cl_2 impinges on surface. Electron harpoons to proximal Cl. (b) Image stabilization/acceleration. (c) Remote dissociation followed by abstraction of Cl^- and hyperthermal ejection of Cl into the gas phase.

the lowest exit Cl energy ($E_{inc}=0.11$ eV, $\Phi_{inc}=40°$) the exit Cl is accelerated vs the incident Cl_2 from 535 m/s to 690 m/s.

The distinct behavior of the ejected Cl from glancing incident angle Cl_2 indicates a separate reaction channel between high and low incident energy Cl_2. The energy of the abstracted Cl products is reduced from ~0.21 eV to ~0.10 eV when the surface is tilted from normal to 40° incident angle for 0.11 eV Cl_2. Trapping in precursor states often scales with the normal component of the incident energy.[42] Tilting the surface lowers the normal component of the incident energy, thereby increasing the precursor channel at the expense of the direct channel. We propose that one abstraction channel is direct and the second abstraction channel is precursor-mediated.

4. Surface temperature experiment

The surface tilt experiment is repeated at high T_S of 500 K. The same 0.65 eV [Fig. 10(a)], 0.27 eV [Fig. 10(b)], and 0.11 eV [Fig. 10(c)] incident energy Cl_2 beams are used. Comparison of the 100 K and 500 K surface tilt data shows clear differences at glancing incident angles. For 0.65 eV incident Cl_2 [Fig. 10(a)], the Cl exit energy is nearly independent of both surface temperature and exit angle, which is consistent with a direct chemisorption mechanism. However, for 0.11 eV incident Cl_2 [Fig. 10(c)], at glancing incident/exit angles, the Cl exit energy increases by a factor of 2 when increasing the surface temperature from 100 K to 500 K. A similar, though less pronounced, effect is seen for 0.27 eV incident Cl_2. This is consistent with the existence of two chemisorption mechanisms for low energy Cl_2. Elevated surface temperatures remove the trapping channel for Cl_2; therefore, only the direct abstracted product is seen. In the sticking experiment, low surface temperature and low incident energy enhance the sticking of Cl_2 on Al(111) consistent with a precursor state. Lower energy ejected Cl from the precursor-mediated channel scales with both surface temperature and normal incident energy.

IV. DISCUSSION

A. Direct abstractive chemisorption

A simple model is proposed for the abstractive chemisorption of Cl_2 on Al(111) at low coverage. (1) The hyperthermal velocity of the ejected Cl is indicative of a vertical electron harpooning event. (2) The velocity of the direct channel is independent of incident parameters at most conditions. (3) A precursor-mediated channel is enhanced at low surface temperature and low incident energy.

As the Cl_2 approaches the Al(111) surface, the dominant reaction at most experimental conditions is direct, abstractive chemisorption. This mechanism is similar to that proposed by NNL, with the exception that only one electron is transferred, leading to neutral ejection. In Fig. 11(a), an incident Cl_2 molecule approaches the surface with varied translational energy. At a distance dependent upon the work function of the Al(111) metal surface and the vertical electron affinity of the Cl_2 in the gas phase [Eq. (1)], an electron may tunnel through vacuum to the Cl_2.

When Cl_2 is suddenly converted to the molecular Cl_2^- ion, a positive image charge is created on the surface [Fig.

11(b)]. The electrostatic attraction between the anion and the image charge on the surface accelerates the Cl_2^- toward the surface. Simultaneously, rapid dissociation of the Cl_2^- anion occurs as it is accelerated toward the surface. The dissociation is driven by the placement of the Cl_2^- high on the repulsive wall of the Cl_2^- potential energy curve following the vertical transition from the neutral Cl_2 potential energy curve [Fig. 1(d)]. The result is shown in Fig. 11(c). The resulting Cl^- anion from the remote dissociation continues toward the surface and chemisorbs. The neutral fragment Cl atom is ejected from the surface at velocities which can exceed the velocity of the incident Cl_2.

This simple model is complicated by the orientation of the impinging Cl_2 molecule with respect to the surface normal, the acceleration of the Cl_2^- anion post harpooning, and the partitioning of the Cl_2^- dissociation energy. The effect of orientation on abstractive chemisorption has been calculated by Binetti *et al.*[43] for O_2/Al(111); similar effects should occur for Cl_2/Al(111). For side-on impinging Cl_2 being harpooned, the energy released in the dissociation of the Cl and Cl^- is most likely directed parallel to the surface, nearly precluding abstractive chemisorption because escape from the surface of either the Cl or Cl^- cannot proceed without energy directed along the surface normal.

End-on impinging Cl_2 is likely to result in hyperthermally ejected Cl and is shown in Fig. 11. In this conformation, as the Cl_2^- breaks apart, it is likely that the charge remains on the halogen atom closest to the surface because it will have the strongest attraction to its image charge. Brandt *et al*. have experimentally demonstrated that orientation of the N_2O with the O-end toward the surface greatly enhances exoelectron emission and N_2 scattering in the N_2O/Cs[12,44,45] and N_2O/Li[12,44,45], systems. Harpooning of an electron from the metal surface to the O atom leads to dissociation of the N_2O into O^- and N_2 fragments. The O^- fragment is accelerated toward the surface by its image charge leading to exoelectron emission. The N_2 fragment scatters back into the gas phase. N-end impinging N_2O places the O atom sufficiently far from the surface to drastically reduce the harpooning probability. Similarly, it is likely that end-on Cl_2 impinging upon the Al(111) surface produces an anionic Cl^- directed at the surface and a neutral Cl directed away from the surface.

For the direct chemisorption channel, the sticking probability is activated. This is quite surprising. Instead, one would expect that when the Cl_2 approaches the surface, all of the molecules would undergo harpooning and subsequently either dissociate or abstractively chemisorb. A similar counterintuitive result is observed for the O_2 chemisorption on Al(111) via electron harpooning: the chemisorption of O_2 is activated and very small ($<1\%$) at low translation energy.[43] For O_2, the activated chemisorption cannot be explained with a simple adiabatic model. Instead, Binetti *et al.*[43] show that the activation barrier is due to the charge transfer being nonadiabatic, very close to the surface, and a strong function of molecular orientation. While an end-on orientation is most favorable for charge transfer, as the incident energy increases, the range of angles increases for charge transfer so the sticking probability increases. Binetti *et al.* explain that incident translational energy increases charge transfer because as the molecule approaches the surface (a) its bond becomes elongated providing better overlap with the negative molecular ion potential and (b) the neutral can become reoriented during its collision with the surface into a more favorable orientation for charge transfer. Elongation and reorientation are significant because charge transfer occurs when the O_2 is so close to the surface that the gas-surface potential is repulsive.

Compared to O_2, charge transfer to Cl_2 should occur slightly further from the surface since Cl_2 has a larger vertical electron affinity; therefore, one must be cautious in assuming an identical mechanism for Cl_2 in the absence of calculations. However, Katz *et al.*[46] have modeled the charge transfer to I_2 during collisions with diamond which should occur further from the surface than charge transfer between Cl_2 and Al(111). They observe an exponential increase in charge transfer events with incident translation energy if the charge transfer occurs when the molecule is on the repulsive portion of the gas-surface potential. This strongly suggests that the Cl_2 direct sticking probability is activated because charge transfer occurs on the repulsive portion of the gas-surface potential. Our simple jellium model calculations show that resonant vertical charge transfer occurs at only 1.1 Å from the surface so it is not unreasonable that charge transfer occurs on the repulsive portion of the gas-surface potential.

B. Precursor-mediated abstractive chemisorption

At low surface temperature and low Cl_2 incident translational energy, a precursor-mediated channel is observed [Fig. 12(a)]. The experimental data that prove the existence of a second abstractive chemisorption channel via a precursor state are: (a) the sticking probability increases with decreasing surface temperature at low incident translation energy and (b) at low surface temperature and low Cl_2 incident translation energy, the ejected Cl atoms have a lower kinetic energy than for direct abstractive chemisorption. We propose that the precursor state is trapping into a shallow physisorption well. In contrast to the direct mechanism, where the electron harpoons to the incident Cl_2 as it approaches the Al(111) surface, the precursor-mediated charge transfer [Fig. 12(b)] proceeds after adsorption to the surface in a loosely bound physisorption state. Recently, Yourdshahyan *et al.* have performed DFT calculations which propose a similar precursor-mediated mechanism in the O_2/Al(111) system.[47] The distance of van der Waals bonding is equal to or greater than the harpooning distance. Since the van der Waals forces are weak and should not strongly affect the Cl_2 potentials, we propose that electron harpooning can proceed after physisorption. Cl_2 physisorbed on the surface is expected to reside in a side-on conformation.[48–50] Cl_2 chattering vibrations or other perturbations on the surface could rapidly lead to the preferred end-on conformation for charge transfer.[47,51,52] Since the range of orientations for Cl_2 undergoing precursor-mediated abstractive chemisorption is very likely to be distinct from Cl_2 undergoing direct abstractive chemisorption, it is reasonable that the two channels should have distinct velocity distributions.

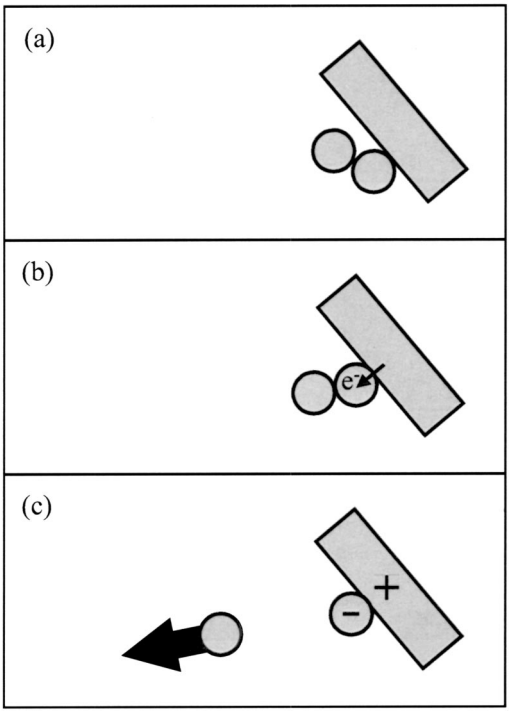

FIG. 12. Schematic diagram of indirect, precursor-mediated electron transfer. (a) Cl_2 is physisorbed on the Al(111) surface. (b) Perturbation of physisorbed Cl_2 on the surface, e.g., chattering vibration, results in favorable conformation for charge transfer. (c) Dissociation of Cl_2^- into chemisorbed Cl^- and hyperthermal ejection of Cl into the gas phase.

The ratio of the mean product velocity to the FWHM of the TOF for both direct and precursor channels also exhibit distinct behavior. The mean velocity to FWHM of the 0.11 eV incident beam at 40° incident angle from a 100 K surface yielded a ratio of ~1.38. This narrow distribution indicates either that a narrow range of orientations produce hyperthermal ejected product or that the electron harpoons onto a shallow portion of the Cl_2^- potential. In contrast, the ratio of ~0.84 for the direct channel indicates a broad distribution. This difference in mean velocity to FWHM is consistent with the existence of distinct direct and precursor-mediated mechanisms.

The work of several groups suggest that Cl_2 molecular precursors exist on the Al surface. However, since only stable precursors can be experimentally probed, these experiments usually only observe the ionisorption states. Smith[53] has shown that Cl_2 adsorbs in a molecular precursor state prior to dissociation and subsequent atomic Cl adsorption on vapor deposited Al films. Bermudez and Glass[54] elaborated on Smith's work by measuring the work function change of the Al(111) surface vs Cl_2 exposure. They suggested that negative Cl^- or Cl_2^- species are formed above the surface. In a similar system, Shi and Jacobi report the existence of O_2^- on the Cs/Ru(001) surface.[55]

Precursor-mediated charge transfer has been seen in the O_2 on oxygen precovered, Cs-covered Ru(0001) system at high oxygen coverage by Grobecker and co-workers.[8,9] We propose that in the Cl_2/Al(111) system, hyperthermal atom abstraction can proceed via a similar precursor-mediated channel with the caveat that the sticking probability data strongly suggests that the Cl_2/Al(111) precursor is a physisorption state. No long time Cl atom ejection is seen in contrast to the very long persistence of exoelectron emission in O_2 on oxygen precovered, Cs-covered Ru(0001). This is consistent with our hypothesis that the precursor for abstractive chemisorption of Cl_2/Al(111) is a metastable physisorption state, not a long-lived ionisorption state.

Although there are no published calculations for Cl_2/Al(111), Weisse *et al.*[56] have calculated a model for O_2/Al(111) to fit the experimental data of the sticking probability for O_2/Al(111). Weisse *et al.* proposed that there is a shallow (0.1 eV) well outside the activation barrier to dissociation which affects the angular dependence of the sticking probability. Because charge transfer probably takes place on the repulsive portion of the O_2–Al(111) potential, it is reasonable that a physisorption well exists at a greater distance from the surface. For Cl_2, the charge transfer also probably occurs on the repulsive portion of the potential because the direct sticking probability is activated, therefore it is also reasonable that a physisorption well exists.

Although our data is consistent with a physisorption precursor, the temperature dependence of the sticking probability of Cl_2/Al(111) at low surface temperature could be due to energy dissipation and stabilization of Cl_2^-. Because Cl_2^- is a stable molecular ion, if the Cl_2 bond were stretched by the interaction with Al(111), it is possible that a vertical electron transfer would occur to a region of the Cl_2^- potential below the vacuum level. This would create metastable Cl_2^- on Al(111). In the absence of physisorption, it is difficult to see how raising the surface temperature would decrease sticking and increase inelastic scattering even if metastable Cl_2^- formation occurs. However, the work of Katz *et al.*[57] for O_2 on Al, Cs, and Ag shows that the seam crossing between the neutral and ionic potentials are complicated and that recrossing can occur. Therefore, it is hard to completely eliminate the possibility that our data for Cl_2/Al(111) sticking is consistent with a Cl_2^- precursor state. However, we feel that it is reasonable to assume that the increase in sticking probability at low-incident energy with decreased surface temperature is most conservatively explained by a Cl_2 physisorption state, and this is consistent with the most recent calculations and data for O_2/Al(111).[56]

C. Comparison to other abstraction studies

In addition to previous work by Kummel and co-workers,[26,27,58–62] halogen atom abstraction has been seen in the F_2/Si(100)-(2×1) system by Li *et al.*[19] and in the Cl_2/K system by Strömquist *et al.*[20] Notably, Tate *et al.*[21,22] have reported that the reaction of F_2 on the Si(100) surface exhibits hyperthermal neutral ejection. F_2 molecules impinging upon the Si surface at 395 m/s produced scattered F atoms with velocities of 1195 m/s. However, the energy for this hyperthermal ejection has been ascribed to the formation of a single Si–F covalent bond and the subsequent repulsion of the second F atom, not harpooning.[63]

D. Conclusion

The reaction of Cl_2 on the Al(111) surface proceeds via a vertical electron harpooning mechanism. Following the electron transfer, one Cl atom is chemisorbed on the surface while the other Cl is ejected into the gas phase. The measured velocity of this atom far exceeds the velocity of the incident Cl_2, consistent with a vertical electron-harpooning mechanism. Moreover, two distinct reaction pathways are capable of producing hyperthermal Cl. The direct abstractive chemisorption can result in ejected Cl velocities which are twice that of the incident Cl_2. A secondary process also results in hyperthermal Cl ejection from a precursor-mediated channel.

[1] B. Kasemo and L. Wallden, Surf. Sci. **53**, 393 (1975).
[2] J. K. Norskov, D. M. Newns, and B. I. Lundqvist, Surf. Sci. **80**, 179 (1979).
[3] B. Kasemo, E. Tornqvist, and L. Wallden, Mater. Sci. Eng. **42**, 23 (1980).
[4] W. S. Struve, J. R. Krenos, D. L. Mcfadden, and D. R. Herschbach, J. Chem. Phys. **62**, 404 (1975).
[5] D. Andersson, B. Kasemo, and L. Wallden, Chem. Phys. Lett. **111**, 593 (1984).
[6] D. Andersson, B. Kasemo, and L. Wallden, Surf. Sci. **152**, 576 (1985).
[7] B. Kasemo, E. Tornqvist, J. K. Norskov, and B. I. Lundqvist, Surf. Sci. **89**, 554 (1979).
[8] R. Grobecker, H. Shi, H. Bludau, T. Hertel, T. Greber, A. Bottcher, K. Jacobi, and G. Ertl, Phys. Rev. Lett. **72**, 578 (1994).
[9] R. Grobecker, T. Greber, A. Bottcher, and G. Ertl, Phys. Status Solidi A **146**, 259 (1994).
[10] L. Hellberg, J. Stromquist, B. Kasemo, and B. I. Lundqvist, Phys. Rev. Lett. **74**, 4742 (1995).
[11] T. Greber, A. Morgante, S. Fichtnerendruschat, and G. Ertl, Surf. Rev. Lett. **2**, 273 (1995).
[12] M. Brandt, T. Greber, N. Bowering, and U. Heinzmann, Phys. Rev. Lett. **81**, 2376 (1998).
[13] T. Greber, Chem. Phys. Lett. **222**, 292 (1994).
[14] T. Greber, Appl. Phys. A: Mater. Sci. Process. **67**, 701 (1998).
[15] B. Gergen, H. Nienhaus, W. H. Weinberg, and E. W. McFarland, Science **294**, 2521 (2001).
[16] J. W. Gadzuk, Comments At. Mol. Phys. **16**, 219 (1985).
[17] T. Greber, Surf. Sci. Rep. **28**, 3 (1997).
[18] T. Greber, Curr. Opin. Solid State Mater. Sci. **3**, 446 (1998).
[19] Y. L. Li, D. P. Pullman, J. J. Yang *et al.*, Phys. Rev. Lett. **74**, 2603 (1995).
[20] J. Stromquist, L. Hellberg, B. Kasemo, and B. I. Lundqvist, Surf. Sci. **352**, 435 (1996).
[21] M. R. Tate, D. Gosalvez-Blanco, D. P. Pullman, A. A. Tsekouras, Y. L. Li, J. J. Yang, K. B. Laughlin, S. C. Eckman, M. F. Bertino, and S. T. Ceyer, J. Chem. Phys. **111**, 3679 (1999).
[22] M. R. Tate, D. P. Pullman, Y. L. Li, D. Gosalvez-Blanco, A. A. Tsekouras, and S. T. Ceyer, J. Chem. Phys. **112**, 5190 (2000).
[23] J. Schochlin, K. P. Bohnen, and K. M. Ho, Surf. Sci. **324**, 113 (1995).
[24] T. F. Hanisco, C. Yan, and A. C. Kummel, J. Chem. Phys. **95**, 6178 (1991).
[25] T. F. Hanisco and A. C. Kummel, J. Phys. Chem. **95**, 8565 (1991).
[26] K. A. Pettus, T. S. Ahmadi, E. J. Lanzendorf, and A. C. Kummel, J. Chem. Phys. **110**, 4641 (1999).
[27] K. A. Pettus, P. R. Taylor, and A. C. Kummel, Faraday Discuss. **117**, 321 (2000).
[28] S. Bashkin and J. O. Stoner, *Atomic Energy Levels and Grotrian Diagrams* (North–Holland, Amsterdam, 1975).
[29] S. Arepalli, N. Presser, D. Robie, and R. J. Gordon, Chem. Phys. Lett. **118**, 88 (1985).
[30] M. Heaven, T. A. Miller, R. R. Freeman, J. C. White, and J. Bokor, Chem. Phys. Lett. **86**, 458 (1982).
[31] S. D. Peyerimhoff and R. J. Buenker, Chem. Phys. **57**, 279 (1981).
[32] K. Aarset, Q. Shen, H. Thomassen, A. D. Richardson, and K. Hedberg, J. Phys. Chem. A **103**, 1644 (1999).
[33] R. J. A. A. Janssen, A. W. Kolfschoten, and G. N. A. Vanveen, Appl. Phys. Lett. **52**, 98 (1988).
[34] T. A. Cleland and D. W. Hess, J. Vac. Sci. Technol. B **7**, 35 (1989).
[35] D. A. Danner and D. W. Hess, J. Appl. Phys. **59**, 940 (1986).
[36] N. N. Efremow, M. W. Geis, R. W. Mountain, G. A. Lincoln, J. N. Randall, and N. P. Economou, J. Vac. Sci. Technol. B **4**, 337 (1986).
[37] P. Klaeboe, E. Rytter, and C. E. Sjogren, J. Mol. Struct. **113**, 213 (1984).
[38] D. A. King and M. G. Wells, Surf. Sci. **29**, 454 (1972).
[39] D. A. King and M. G. Wells, Proc. R. Soc. London, Ser. A **339**, 245 (1974).
[40] B. Berenbak, D. A. Butler, B. Riedmuller, D. C. Papageorgopoulos, S. Stolte, and A. W. Kleyn, Surf. Sci. **414**, 271 (1998).
[41] F. M. Zimmermann and W. Ho, Surf. Sci. Rep. **22**, 129 (1995).
[42] C. R. Arumainayagam and R. J. Madix, Prog. Surf. Sci. **38**, 1 (1991).
[43] M. Binetti, O. Weisse, E. Hasselbrink, G. Katz, R. Kosloff, and Y. Zeiri, Chem. Phys. Lett. **373**, 366 (2003).
[44] M. Brandt, T. Greber, F. Kuhlmann, N. Bowering, and U. Heinzmann, Surf. Sci. **404**, 160 (1998).
[45] M. Brandt, F. Kuhlmann, T. Greber, N. Bowering, and U. Heinzmann, Surf. Sci. **439**, 49 (1999).
[46] G. Katz, Y. Zeiri, and R. Kosloff, Chem. Phys. Lett. **358**, 284 (2002).
[47] Y. Yourdshahyan, B. Razaznejad, and B. I. Lundqvist, Phys. Rev. B **65**, 075416 (2002).
[48] M. F. Toney and S. C. Fain, Phys. Rev. B **36**, 1248 (1987).
[49] K. M. Hock and R. E. Palmer, J. Chem. Phys. **97**, 8736 (1992).
[50] G. H. Lushington and C. F. Chabalowski, J. Mol. Struct.: THEOCHEM **544**, 221 (2001).
[51] B. I. Lundqvist, A. Bogicevic, K. Carling *et al.*, Surf. Sci. **493**, 253 (2001).
[52] Y. Yourdshahyan, B. Razaznejad, and B. I. Lundqvist, Solid State Commun. **117**, 531 (2001).
[53] T. Smith, Surf. Sci. **32**, 527 (1972).
[54] V. M. Bermudez and A. S. Glass, J. Vac. Sci. Technol. A **7**, 1961 (1989).
[55] H. Shi and K. Jacobi, Surf. Sci. **303**, 67 (1994).
[56] O. Weisse, C. Wesenberg, M. Binetti, E. Hasselbrink, C. Corriol, G. R. Darling, and S. Holloway, J. Chem. Phys. **118**, 8010 (2003).
[57] G. Katz, Y. Zeiri, and R. Kosloff, Surf. Sci. **425**, 1 (1999).
[58] A. J. Komrowski, K. Ternow, B. Razaznejad *et al.*, J. Chem. Phys. **117**, 8185 (2002).
[59] A. J. Komrowski, J. Z. Sexton, A. C. Kummel, M. Binetti, O. Weisse, and E. Hasselbrink, Phys. Rev. Lett. **87**, 246103 (2001).
[60] Y. Liu, A. J. Komrowski, P. R. Taylor, and A. C. Kummel, J. Chem. Phys. **109**, 2467 (1998).
[61] M. Binetti, O. Weisse, E. Hasselbrink, A. J. Komrowski, and A. C. Kummel, Faraday Discuss. **117**, 313 (2000).
[62] M. Binetti, O. Weisse, E. Hasselbrink, A. J. Komrowski, and A. C. Kummel, Abstr. Pap. - Am. Chem. Soc. **221**, U312 (2001).
[63] L. E. Carter, S. Khodabandeh, P. C. Weakliem, and E. A. Carter, J. Chem. Phys. **100**, 2277 (1994).